ASIAN JOURNAL OF CIVIL ENGINEERING (BHRC) VOL. 16, NO. 5 (2015)
PAGES 709-732

A NEW MODIFICATION IN DECOUPLED SCALED BOUNDARY METHOD WITH DIAGONAL COEFFICIENT MATRICES FOR ANALYSIS OF 2D ELASTOSTATIC AND TRANSIENT ELASTODYNAMIC PROBLEMS

M.I. Khodakarami* and M. Fakharian
Faculty of Civil Engineering, Semnan University, P.O. Box 35131-19111, Semnan, Iran

Received: 12 February 2015; **Accepted:** 16 April 2015

ABSTRACT

The scaled boundary based methods are commonly known as semi-analytical approaches, which have very good accuracy and efficiency for solving various kinds of problems. In this paper, a new trend for improvement of the decoupled scaled boundary-finite element method (DSBFEM) in order to solve the 2D elastostatic and elastodynamic problems is provided. In this technique, only the boundaries of the problem domain are discretized by specific sub-parametric elements. Mapping functions are employed as a class of higher-order Lagrange polynomials which are set at Gauss-Lobatto-Legendre control points,so, the special shape functions, Gauss-Lobatto-Legendre numerical integration, and the integral form of the weighted residual method lead to the diagonal coefficient matrices in the governing equations. The main differences between the study conducted and the prior researches regarding decoupled scaled boundary-finite element method is that here in, geometry production procedure of the interpolation function, integration of the different is selected, and using this approach, we could reduce the complexity of the DSBFEM. Validity and accuracy of the present method are demonstrated through two benchmark elastostatic problems and three benchmark elastodynamic problems that are successfully modeled using a few numbers of DOFs. The numerical results agree very well with the analytical solutions and the results from other numerical methods.

Keywords: Decoupled SBFEM; 2D elastic problems; sub-parametric element; Lagrange polynomials; Gauss-Lobatto-Legendre integration.

1. INTRODUCTION

Various classes of numerical methods such as Finite Element Methods (FEM), Boundary

*E-mail address of the corresponding author: khodakarami@semnan.ac.ir (M.I. Khodakarami)

Element Methods (BEM), and Scaled Boundary based Methods (SBFEM), and mesh-less methods are usually used in order to solve the elastostatic and elastodynamic problems in two-dimensional domains (see, Fig. 1).

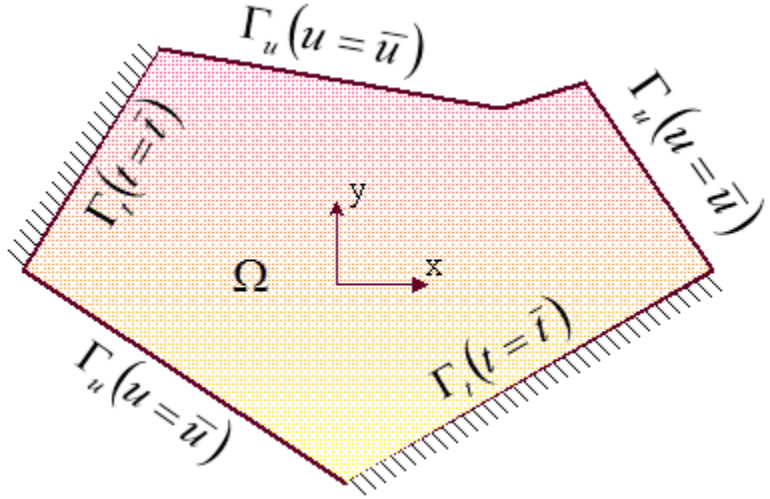

Figure 1. A two-dimensional domain (Ω) with Dirichlet (Γ_u) and Neumann (Γ_t) boundry conditions for elastostatic and elastodynamic problems

The use of FEM is advantageous as its procedures are well established in [1, 2]. The researchers in [3-6] have presented a new numerical solution approach based on the FEM, which can be used for solving some 2D elastostatic and elastodynamic problems.

Another desirable method for solving elastic problems is the boundary element (BE) based methods in which require reduced surface discretizations and so fewer unknowns are needed to be stored. Moreover, BEM requires a fundamental solution for the governing differential equation in the domain in order to obtain the boundary integral equation; in these conditions, the coefficient matrices of BEM are much smaller than those of FEM, routinely non-positive definite, non-symmetric, and fully populated (for example, see [7-12]). In [13, 14], a coupling of the FEM and the BEM are used for solving elastodynamic problems. Time domain FEM/BEM coupling formulation for the 2D elastodynamic problem has been presented in [15]. Soares and Mansur [16, 17] have described a procedure to improve the stability and efficiency of time-domain BEM for wave problems. An efficient FEM/BEM coupling method for elastodynamic problems in time domain has been described in [18]. Abreu et al. [19] have presented a numerical method based on the BEM and the CQM to solve wave propagation problems. Carrer et al. [20] have developed a D-BEM approach for the solution of 2D wave propagation problems. An efficient time-truncation approach applied to the boundary element solution of 2D out-of plane elastodynamic problems has been presented in [21].

During the last decades, researchers have also paid attention to mesh-less methods. These methods routinely do not require specific meshes, while the boundary nodes are usually needed. Several mesh-less methods have been reported in the literature among which, mesh-less local Petrov-Galerkin method [22, 23], boundary element-free method [24], local point

interpolation method [25], local boundary integral equation method [26], collocation method [27], hybrid method [28], and other mesh-free methods [29, 30] have been employed in the modeling of elastodynamic problems.

Combining the advantages of FEM and BEM, SBFEM was successfully developed [31]. Using surface finite elements, SBFEM discretizes only the boundary of the domain by transforming the governing partial differential equations to ordinary differential equations, which may be solved analytically. SBFEM, which requires no fundamental solution, have also been employed for the analysis of elastostatic problems and elastodynamic problems (for example, see [32] and [33], respectively). Some wave propagation problems in non-homogeneous elastic domains have been solved using the SBFEM [34].

Researchers in [35] have been developed SBFEM based approach for numerical analysis of 2-D elastic systems with rotationally periodic (and/or cyclic) symmetry under arbitrary load conditions. Issues relating to the practical implementation of the coupled boundary element–scaled boundary finite element method are addressed in [36]. In [37], researchers have been developed a mesh-less method for determining the shape functions in the circumferential direction based on the local Petrov-Galerkin approach, as increased smoothness and continuity of the shape functions is obtained, and the solution is shown to converge significantly faster than conventional scaled boundary finite elements. SBFEM is employed in [38] in order to derive an equation for the displacement unit-impulse response matrix on the near field/far field interface; in this research, an efficient method for modeling the propagation of elastic waves in layered media is developed. A new proposed approach using SBFEM is based on a piecewise linear approximation of the first derivative of the displacement unit-impulse response matrix and has been applied to soil–structure interaction problems involving scalar and vector waves is studied in [39].

A formulations of the smoothed polygonal FEM with simple averaging technique and the scaled boundary polygon formulation in [41] and [42] investigates the concepts of isogeometric analysis and the scaled boundary finite element method (SBFEM) are combined. Application of the Fourier shape functions in the SBFEM to form the approximation in the circumferential direction has been studied in [43].

A modification of the scaled boundary finite element method with diagonal coefficient matrices (DSBFEM) has been proposed in [44] for solving potential problems and it is applied to solve elastostatic problems [45]. Also the proposed method is used to solve elastodynamic problems in [46, 48]. Moreover it is also the method to solve the three-dimensional elastostatic problems [47] and an infinite half-space problems is used [48]. DSBFEM is utilized for solution of two-dimensional elastodynamic problems in the frequency domain by employing Fast Fourier Transform in [40].

In this study, we improved the efficiency and reduced complexity of the semi-analytical based on the scale boundaries approach so called decoupled scaled boundary-finite element method (DSBFEM) which had been proposed in [44-48]; where, the Lagrange polynomials is used as mapping functions instead of Chebyshev polynomials and also Gauss-Lobatto-Legendre quadrature is employed instead of Clenshaw-Curtis integration technique in order to calculate the coefficient matrices. By the way, with implementing this technique, the governing equations for each node are independent of the other nodes and this will reduce the computational costs; because evaluation of matrices and vectors and obtaining the solution procedure is more easier while one employs Lagrange polynomial and GLL

quadrature. Accuracy of the present method is demonstrated through five benchmark problems and its results are shown a good agreement between this approach and other methods.

2. SUMMARY OF DECOUPLED SCALED BOUNDARY FINITE-ELEMENT METHOD

The derivation of the decoupled scaled boundary finite-element method (DSBFEM) for various kinds of engineering problems is detailed in [44-48] and here in, only the concept and the equations necessary for explaining the new developments in this research are summarized.

In the DSBFEM, a local-coordinates-origin (LCO) is chosen from which all boundaries of the domain are visible (as shown in Fig. 2). In this method, only the boundaries that do not pass through the LCO should be discretized into n_e one-dimensional (for a two-dimensional problem) using higher-order sub-parametric elements, so that. As shown in Fig. 2, the global Cartesian coordinates in 2D problems are ($\hat{x}, \hat{y}$), in which using the Lagrange polynomials would be transmitted into local coordinates (ξ, η); where, ξ is radial co-ordinate from the LCO ($\xi = 0$) to the boundaries ($\xi = 1$) and η is the tangential co-ordinate which varies between -1 and +1 on the boundaries. Each element on the boundary is analogous to a line; the geometry of an element ($\{x(\eta)\} = [x \quad y]^T$) is interpolated using these of mapping functions $[\Phi(\eta)]$, as,

$$\{x(\eta)\} = [\Phi(\eta)]\{x\}, \tag{1}$$

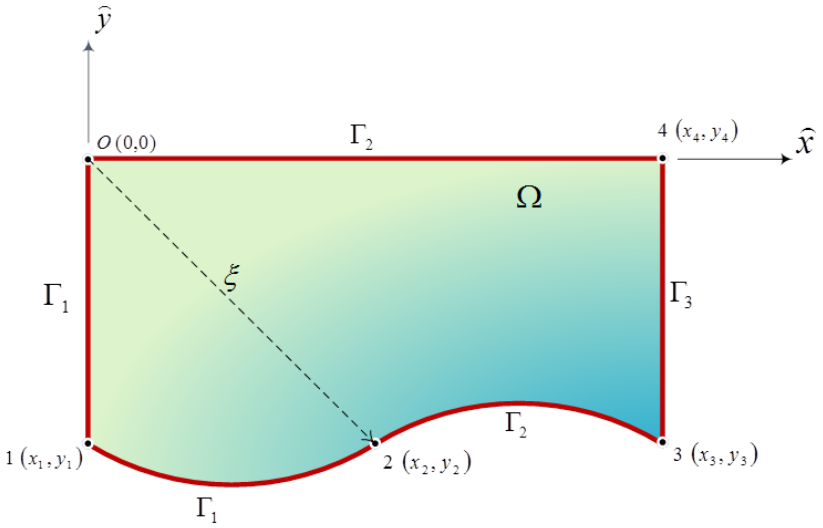

(a)

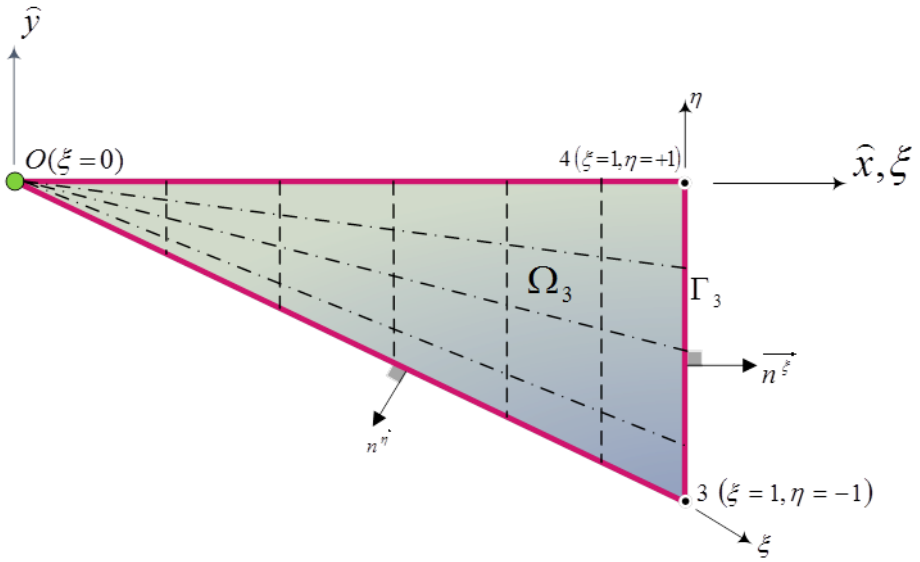

(b)

Figure 2. Modeling of 2D bounded domain, and the LCO: (a) in global coordinates system, and (b) in DSBFEM system for boundary Γ_3 and its related sub-domain Ω_3.

where, $\{x\}=[x \quad y]^T$ denotes the global coordinates of boundary points, $[\Phi(\eta)]$ is a $2n_\eta+1$ matrix and $n_\eta+1$ is number of nodes in the element. Any point in the domain with coordinates $\{\hat{x}(\xi,\eta)\}=[\hat{x}(\xi,\eta) \quad \hat{x}(\xi,\eta)]^T$ relates to the corresponding point on the elements of boundary as

$$\{\hat{x}(\xi,\eta)\}=\xi.\{x(\eta)\}, \tag{2}$$

The mapping functions, which are used in DSBFEM in pervious works [44-48], are higher-order Chebyshev polynomials that interpolate the geometry of the problem using Chebyshev control points.

The differential element of area in the global coordinates ($d\hat{x}d\hat{y}$) is evaluated by a 2×2 Jacobian matrix of the transformation respect to a differential element of area in local coordinates ($d\xi d\eta$) by

$$d\hat{x}d\hat{y}=\xi\left|J(\eta)\right|d\xi d\eta \tag{3}$$

where, $J(\eta)$ indicates the Jacobian matrix may be written in the following form

$$J(\eta)=\begin{bmatrix} x(\eta) & y(\eta) \\ x_{,\eta}(\eta) & y_{,\eta}(\eta) \end{bmatrix}. \tag{4}$$

The spatial derivatives for two coordinate systems are related as

$$\begin{bmatrix} \partial/\partial\,\hat{x} & 0 & \partial/\partial\,\hat{y} \\ 0 & \partial/\partial\,\hat{y} & \partial/\partial\,\hat{x} \end{bmatrix}^T = [b^1(\eta)]\frac{\partial}{\partial\xi} + [b^2(\eta)]\frac{1}{\xi}\frac{\partial}{\partial\eta}, \tag{5}$$

where,

$$[b^1(\eta)] = \frac{1}{|J(\eta)|}\begin{bmatrix} y(\eta)_{,\eta} & 0 \\ 0 & -x(\eta)_{,\eta} \\ -x(\eta)_{,\eta} & y(\eta)_{,\eta} \end{bmatrix}, \tag{6}$$

$$[b^2(\eta)] = \frac{1}{|J(\eta)|}\begin{bmatrix} -y(\eta) & 0 \\ 0 & x(\eta) \\ x(\eta) & -y(\eta) \end{bmatrix}. \tag{7}$$

The unit normal vector along each local coordinates on the boundary may be defined as the following equations

$$[n^{\xi}(\eta)] = \frac{1}{\left|\begin{Bmatrix} y_{,\eta}(\eta) \\ -x_{,\eta}(\eta) \end{Bmatrix}\right|}\begin{bmatrix} y_{,\eta}(\eta) & 0 \\ 0 & -x_{,\eta}(\eta) \\ -x_{,\eta}(\eta) & y_{,\eta}(\eta) \end{bmatrix}, \tag{8}$$

$$[n^{\eta}(\eta)] = \frac{1}{\left|\begin{Bmatrix} -y(\eta) \\ x(\eta) \end{Bmatrix}\right|}\begin{bmatrix} -y(\eta) & 0 \\ 0 & x(\eta) \\ x(\eta) & -y(\eta) \end{bmatrix}. \tag{9}$$

In the DSBFEM, special polynomials $N(\eta)$ are used as shape functions, in order to interpolating the displacement function and its derivatives, across the element; where, these polynomial have two specific characteristics; the shape functions have the property of Kronecker Delta, and their first derivatives are equal to zero at any given control point.

For a $n_\eta + 1$ node element, these shape functions are expressed as a polynomial of degree $2n_\eta + 1$ at ith control point [46]

$$N_i(\eta) = \sum_{m=0}^{2n_\eta+1} a_m \eta^m \ . \tag{10}$$

The displacement field in a two-dimensional problem, $\{u(\xi,\eta,t)\} = \lfloor u_x(\xi,\eta,t) \quad u_y(\xi,\eta,t) \rfloor$ at any point with given (ξ,η) and given time t is obtained by interpolation of the displacement function using these shape functions as

$$\{u(\xi,\eta,t)\} = \lfloor u_x(\xi,t) \quad u_y(\xi,t) \rfloor^T \{u(\xi,\eta,t)\} = [N(\eta)]\{u(\xi)\} \tag{11}$$

In the global coordinates, the strain field in a two-dimensional problem is calculated by

$$\{\varepsilon(x,y,t)\}=\begin{bmatrix}\frac{\partial}{\partial x} & 0 & \frac{\partial}{\partial y}\\ 0 & \frac{\partial}{\partial y} & \frac{\partial}{\partial x}\end{bmatrix}^{T}\{u(x,y,t)\} \tag{12}$$

Using Eqs. (5) and (11), the strain field (Eq. (12)) in local coordinates will be expressed as

$$\{\varepsilon(\xi,\eta,t)\}=\left[B^{1}(\eta)\right]\{u(\xi,t)\}_{,\xi}+\frac{1}{\xi}\left[B^{2}(\eta)\right]\{u(\xi,t)\} \tag{13}$$

where, $[B^1(\eta)] = [b^1(\eta)][N(\eta)]$ and $[B^2(\eta)] = [b^2(\eta)][N(\eta)]_{,\eta}$. As the first derivatives of the shape functions at any nodes are zero, the second term of Eq. (13) at the control points will be vanished and at other point with any (ξ,η), this term is none-zero. The relation between strain and stress may be expressed using Hook's Law and Eq. (13) using the elasticity matrix [*D*] as given by

$$\{\sigma(\xi,\eta,t)\}=[D]\left(\left[B^{1}(\eta)\right]\{u(\xi,t)\}_{,\xi}+\frac{1}{\xi}\left[B^{2}(\eta)\right]\{u(\xi,t)\}\right) \tag{14}$$

In the DSBFEM, as mentioned in previous studies [44], the weak form of governing equations of elastodynamic problems in the local coordinates is expressed as

$$\left[D^{0}\right]\{u(\xi,t)\}_{,\xi\xi}+\frac{1}{\xi}\left[D^{1}\right]\{u(\xi,t)\}_{,\xi}+\{F^{b}(\xi,t)\}=[M]\{u(\xi,t)\}_{,tt} \tag{15}$$

where,

$$[D^{0}]=\int_{-1}^{+1}[B^{1}(\eta)]^{T}[D][B^{1}(\eta)]\,|J(\eta)|\,d\eta \tag{16}$$

$$[D^{1}]=\int_{-1}^{+1}[B^{1}(\eta)]_{,\eta}^{T}[D][B^{2}(\eta)]\,|J(\eta)|\,d\eta \tag{17}$$

$$[M]=\int_{-1}^{+1}[N(\eta)]^{T}\rho[N(\eta)]\,|J(\eta)|\,d\eta \tag{18}$$

$$\{F^{b}(\xi,t)\}=\int_{-1}^{+1}[N(\eta)]^{T}\{f^{b}(\xi,\eta,t)\}\,|J(\eta)|\,d\eta \tag{19}$$

Eq. (15) is the governing equation of elastodynamic problems, is a set of partial differential equations of radial coordinate ξ and time *t*, which represents the governing equation of the DSBFEM for elastodynamic problems; it is clear that for a elastostatic problems the right hand side of Eq. (15) will be vanished and the governing equation is expressed as an ordinary differential equation respect to ξ; calculation of the vectors and matrices of Eq. (15) is obtained using Clenshaw-Curtis quadrature; it is motivated that this

procedure makes these matrices diagonal and the governing equation is decoupled for *i*th degree of freedom in the DSBFEM leads to

$$D_{ii}^{0}.u_{i,\xi\xi}(\xi,t)+\frac{1}{\xi}D_{ii}^{1}.u_{i,\xi}(\xi,t)+F_{i}^{b}(\xi,t)=M_{ii}.u(\xi,t)_{i,tt} \tag{20}$$

3. MODIFICATION OF DSBFEM

The modeling and solution procedure that are used in the present work is similar to the studies which is published in [44-48], else the mapping functions, control points and the numerical integration technique. Here in, against of the previous DSBFEM, a sets of higher-order Lagrange polynomials are used in order to interpolation of the model, and geometry, where these mapping functions are set up on Gauss-Lobatto-Legendre points as control points and employing the Gauss-Lobatto-Legendre quadrature for calculating the matrices, leads to decoupled partial differentials.

3.1 Lagrange polynomials as mapping function

For a $(n_\eta+1)$-node element, a Lagrange polynomial of (n_η) is used, these polynomials for *i*th point will be calculated as [49]

$$\phi_i(\eta)=\prod_{k=1,k\neq i}^{n_\eta+1}\frac{\eta-\eta_k}{\eta_i-\eta_k} \tag{21}$$

Considering Eq. (21), the Lagrange polynomials have the properties of the Kronecker Delta at any control point ($\phi_i(\eta_j)=\delta_{ij}$). As it is clear for preparing an order n_η parent element, $n_\eta+1$ nodes are required, where, two end-nodes are located at the extremity ($\eta=\pm1$) of the element and other $n_\eta-1$ remained internal nodes are located at the Gauss–Lobatto–Legendre points, which are the roots of the first-order derivative of order n_η Legendre polynomial [49]

$$\frac{d}{d\eta}P_{n_\eta}(\eta)=0 \tag{22}$$

where, the Legendre polynomial of order n_η is expressed using Rodrigues' formula[50],

$$P_{n_\eta}(\eta)=\frac{1}{2^n n!}.\frac{d^{n_\eta}}{d\eta^{n_\eta}}\left[\left(\eta^2-1\right)^{n_\eta}\right] \tag{23}$$

For a three-node element, the position of nodes and mapping functions are illustrated in Fig. 3.

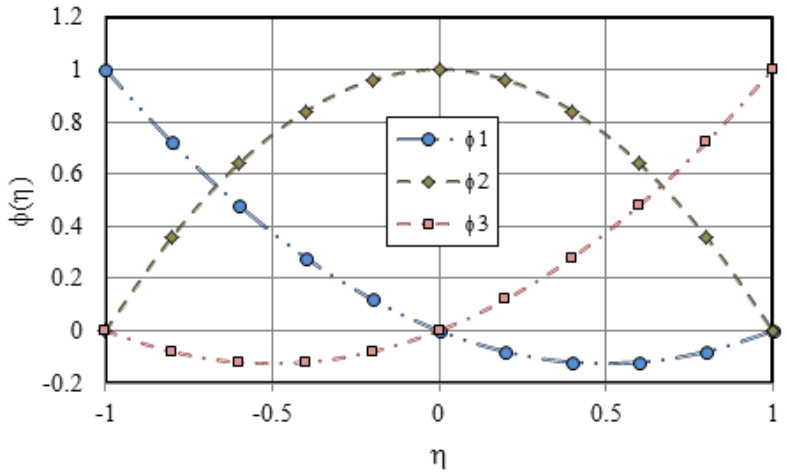

Figure 3. Lagrange interpolation mapping functions of a sample three-node element at the GLL points of reference element

3.2 Gauss-Lobatto-Legendre quadrature

In this study, to calculate the vectors and matrices in Eq. (15), the Gauss-Lobatto-Legendre numerical integration method is applied the numerical integration method, calculates the values of the coefficients matrix in the GLL, according to the node element that corresponds to the points and also features a shape functions used, resulting diagonal matrix of coefficients used in the equation. Weight coefficients used in the method of integration is calculated using the following equation [49]

$$w_i = \frac{2}{n_\eta (n_\eta + 1)(P_{n_\eta}(\eta_i))} \quad ; \quad i = 0,1,2,\ldots,(n_\eta + 1) \tag{24}$$

Consequently, the components of coefficient matrices may be expressed as

$$D_{ij}^0 = \delta_{ij} w_i [B^1(\eta_i)]^T [D][B^1(\eta_i)] \left|J(\eta_i)\right| \tag{25}$$

$$D_{ij}^1 = \delta_{ij} w_i [B^1(\eta_i)]_{,\eta}^T [D][B^2(\eta_i)] \left|J(\eta_i)\right| \tag{26}$$

$$M_{ij} = \delta_{ij} w_i [N(\eta_i)]^T \rho [N(\eta_i)] \left|J(\eta_i)\right| \tag{27}$$

where, δ_{ij} denotes the Kronecker Delta which results in diagonal coefficient matrices. So, the system of partial differential Eq. (15) may be expressed as a single differential equation regarding to a specified point *i* as the following expression

$$D_{ii}^0 . u_{i,\xi\xi}(\xi,t) + \frac{1}{\xi} D_{ii}^1 . u_{i,\xi}(\xi,t) + F_i^b(\xi,t) = M_{ii} . u(\xi,t)_{i,tt} \tag{28}$$

It is worthwhile remarking that Eq. (28) offers a set of ordinary differential equations for an elastostatic problem and elastodynamic problem with 2*n* DOFs. Each differential equation in

Eq. (28) depends only on the elastostatic and elastodynamic function of the *i*th DOF. This means that the coupled system of differential equations has been transformed into decoupled differential equations using a special set of weak formulation procedure, mapping functions, quadrature, and shape functions. In other words, to evaluate the displacement function and its derivatives at a given point, the governing equation that is corresponding to the point should be solved, only. As may be illustrated later, the decoupled differential equations system proposed in this paper can also provide higher rates of convergence by employing a few numbers of DOFs compared to other numerical methods.

4. SOLUTION PROCEDURE

In the DSBFEM, a problem will solved in two steps; the first is solving the governing equation (28) for any DOF which is subjected to external forces (i.e., these forces may be cause of body or surface loads or may be concentrated forces at the nodes) and the stress field at LCO regarding to all these nodes will be calculated. In the second step, the governing equation for all nodes (actually the nodes which the results is considerable at those) is evaluated and after determination of the displacement along radial coordinate (ξ), using the shape functions, displacement and also strain and stress at any internal or boundary points can be given. This approach is done according to following phases:

a) Phase I:

a-i) Read the mechanical and geometrical data, boundary conditions and initial condition and select a suitable location for LCO,

a-ii) Calculate the coefficient matrices ($[D^0]$, $[D^1]$ and [M] using Eqs. (25)-(27)) regarding the geometrical and mechanical properties and force vector ($\{F^b\}$; Eq. (19)) regarding the loads in the problem for each element,

a-iii) Assembling the matrices and vector for all element and obtain the total matrices and force vector,

a-iv) Solve the governing equation (28) with implementing the boundary and initial conditions in order to evaluate the displacement along radial coordinate (ξ) for any node,

a-v) Calculate the total stress ($\{\sigma(\xi,\eta,t)\}$) at LCO by summation of the stresses from step (iv) which is obtained using Eq. (14),

b) Phase II:

b-i) Obtain the force along radial coordinate ($\{F^b\}$) regarding the stress at LCO and external forces at the boundary and loads using Eq. (19) for any boundary nodes,

b-ii) Solve the Eq. (28) along each radial coordinate for each desirable control points and evaluate the displacement field $u_i(\xi,t)$,

b-iii) Evaluating the displacement, strain and stress fields using Eqs. (11), (13) and (14), respectively,

b-iv) Plot the results.

5. NUMERICAL EXAMPLES

The efficiency and accuracy of the proposed new technique evaluated through representative some numerical examples. To this end, a couple of two-dimensional elastostatic problems and three 2D elastodynamic problems are solved in this section. The results obtained from present method are compared to those reported by other numerical methods and/or exact analytical solutions. All quantities are measured in SI units.

5.1 Long cantilever beam subjected to static load

Fig. 4 shows a simple classical plane stress benchmark problem of 2D cantilever which is subjected to a vertical traction at its free end; for this beam, the Young's modulus $E = 2.1\times10^5\ MN/m^2$ and Poisson's ratio $\nu = 0.3$.

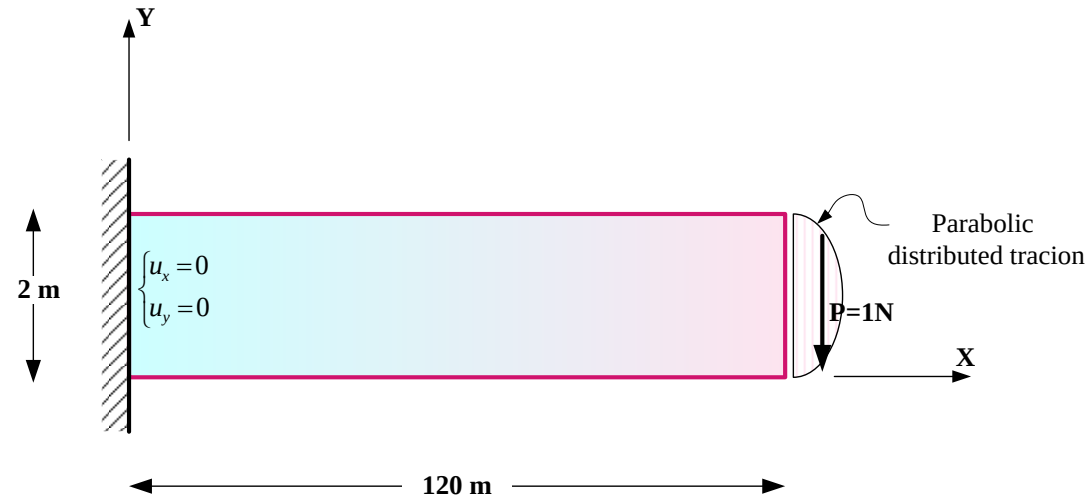

(a)

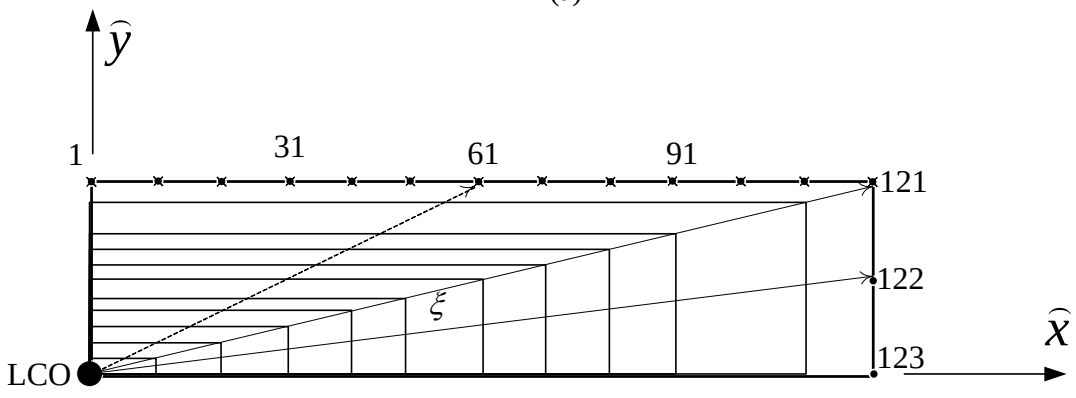

(b)

Figure 4. The first elastostatic example; (a) geometry and boundary conditions in global Cartesian coordinates and (b) the LCO and proposed mesh using 61 three-node one dimensional elements and 246 degree of freedom

The thickness of the beam is unit. In this problem, the LCO is chosen as shown in Fig. 5b and discretization of the problem domain has been done using 61 three-node one-dimensional elements with total 246 DOFs. To calculate the variation of displacement component along the *X*-axis at Y=1.0, after solving the problem in first phase (as described in section 4) it is just necessary to solve the governing equation corresponding to the 122th node. The solution result of this example using the proposed method is shown in Fig. 5; these results are compared with the method used [45] and the results from an analytical solution. It is evident that the result of the present study agrees very well with other solution techniques; furthermore, the contours of variation of u_y and σ_{XX} of this example within the domain using the present method are depicted in Fig. 6a and Fig. 6b, respectively.

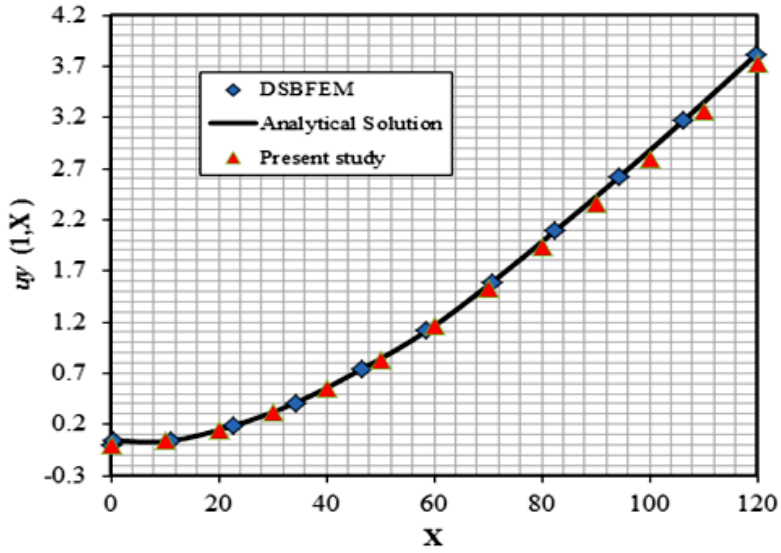

Figure 5. The numerical results and the analytical solution of the vertical displacement of the beam ($u_Y \times 10^4$) of the first example, along the X-axis at Y=1.0 which is evaluated from DSBFEM [45], analytical solution and present study

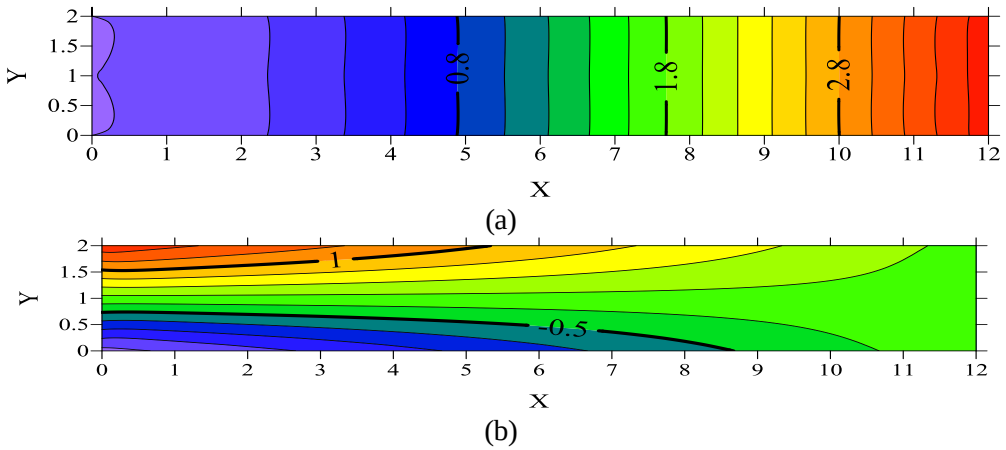

Figure 6. Contour plots for the first example using the proposed technique; (a) u_y and (b) σ_{XX}

5.2 Deep Fixed-fixed end beam

The scope of elastostatic example is to illustrate the accuracy of the proposed approach based on DSBFEM by solving a simple plane stress plate problem, which is clamped at its both ends with a 0.1*m* thickness. The material properties are $E = 2\times10^5\ MN/m^2$ and $\nu = 0.2$. As it is shown in Fig. 8, the beam is under a uniform distributed normal vertical traction of $\sigma_{YY} = -1\ kN/m^2$. The LCO has been selected as shown in Fig. 7b. For this problem, only 4 three-node elements with 18 numbers of DOFs are used. The numerical result of this problem using the present method is shown in Figs. 8 and 9 and these results are compared with the analytical solution and the method used in [45]; this comparison shows a good agreement between the results in the condition that in the present study, the problem is solved using just 9 control points. In addition, the contours of the vertical displacement and horizontal stresses to the space are calculated using the proposed method is shown in Fig. 10.

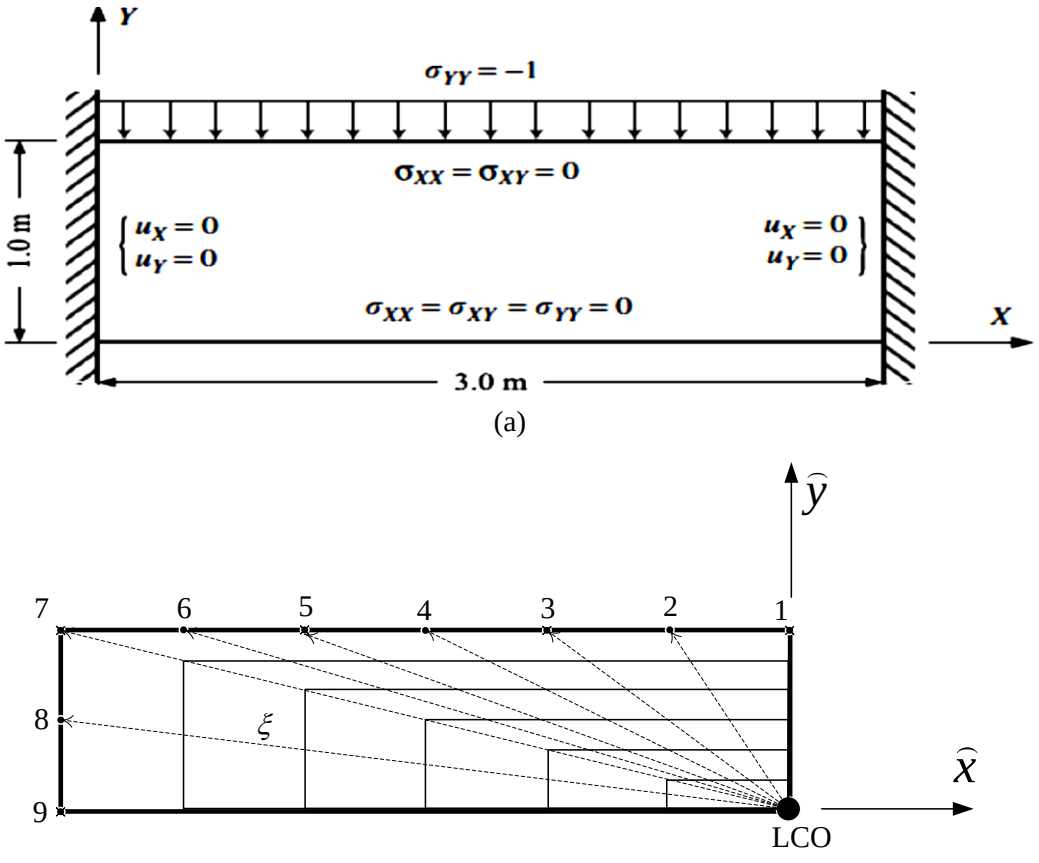

Figure 7. Second elastostatic example; (a) geometry, loads and boundary conditions in global Cartesian coordinates and (b) the place of LCO and meshing with 4 three-node elements with total 18 DOFs

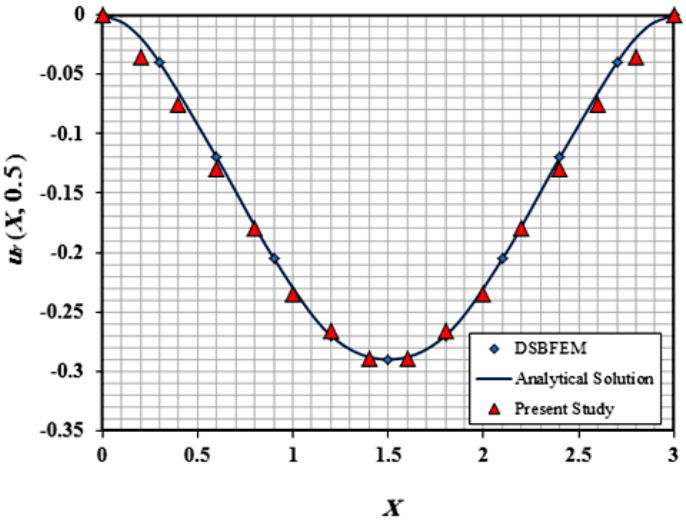

Figure 8. The result solution of second example for the distribution of u_Y along the direction of X at Y=0.5; DSBFEM [45], analytical solution and present technique

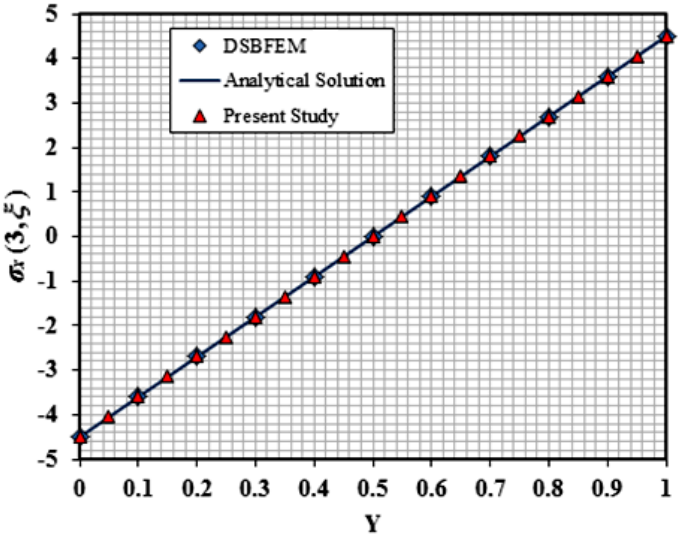

Figure 9. The result solution of second example for the distribution of σ_{XX} u_y along the direction of Y at X=3.0; DSBFEM [45], analytical solution and present technique

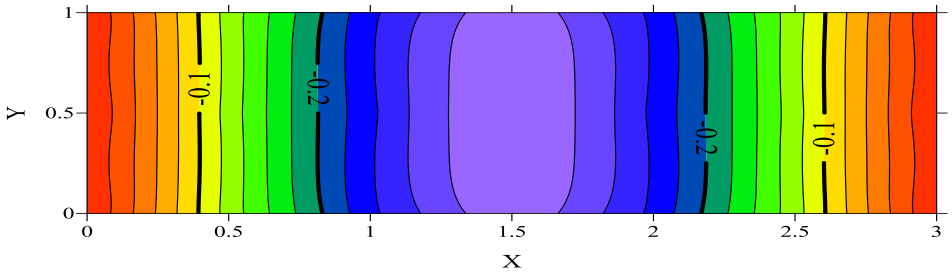

(a)

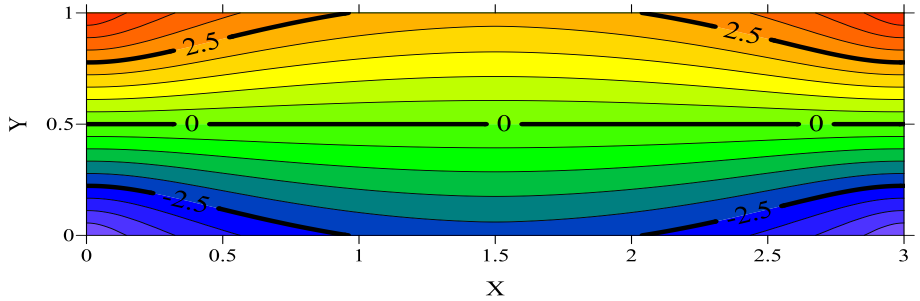

(b)

Figure 10. Contour plots for the second example using the technique in the present study method: (a)u_Y and (b) σ_{XX}

5.3 Cantilever plate under transverse dynamic loading

The first elastodynamic example, 2D wave propagation problem is investigated to verify the proposed method in comparison with other numerical solutions. A cantilever plate (Fig. 11), is under a uniform dynamic traction on its upper side. The triangular function of loading increases from zero at time $t = 0$ to $T_0 = 1\ N/m$ at t = 3sec. and then decreases to zero at $t = 6\ \text{sec}$ The material Young's modulus $E = 1\ N/m^2$, the mass per volume $\rho = 1\ kg/m^3$ and the Poisson's ratio $\upsilon = 0.3$. Modeling of this example is obtained by selecting the LCO at the left-bottom corner of the problem domain and the domain boundaries are discretized using a series of three-node elements with only 7 nodes and 14 total numbers of DOFs, in total (see Fig. 11). The length of the element is chosen as at least 5 nodes placed in the minimum wavelength. In this example, the velocity of the shear wave (v_s) is equal to 0.62 *m*/*sec*., and the velocity of the longitudinal wave (v_L) is equal to 1.16 *m*/*sec*. The dominant frequency of the loading this example $\omega = 3.1\ rad/\text{sec}.$ and the minimum wave length ($\lambda_{\min}$) is regarding to shear wave and equal to 1.25; so, at least five node should be place in this wave length and using a series of three-node elements leads to the elements with the maximum node distance 0.31 *m* and we have chosen a three-node element with length 0.5 *m* for discretizing the geometry of this problem.

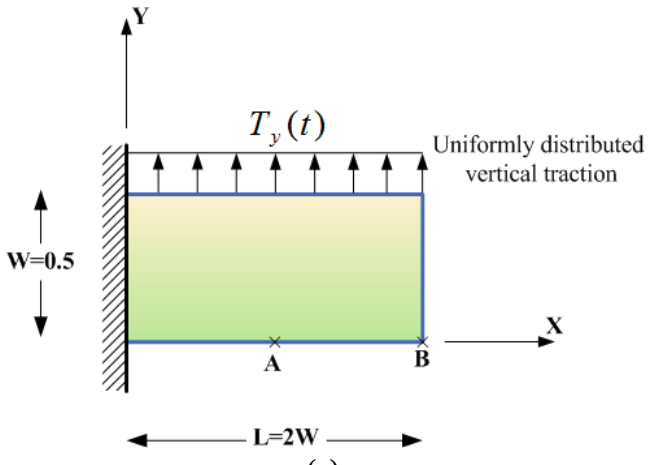

(a)

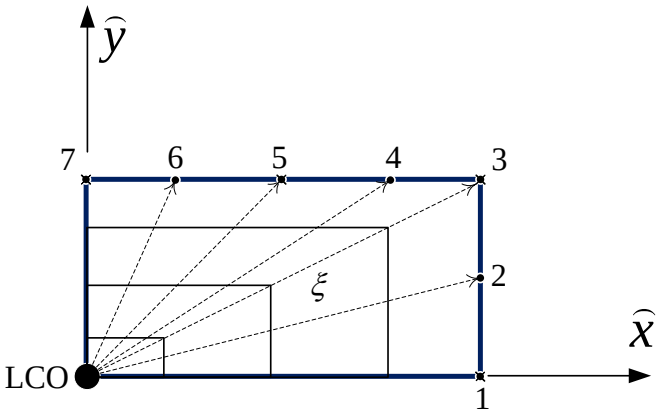

(b)

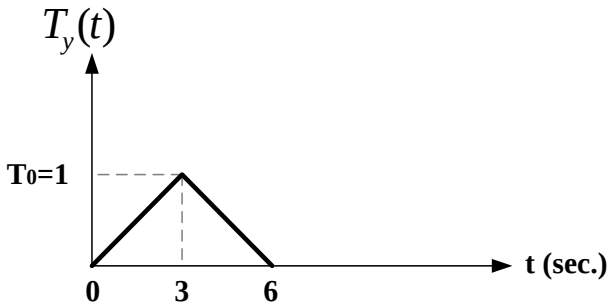

(c)

Figure 11. The third example; 2D plane stress plate; (a) geometry, loading location and boundary conditions in global Cartesian coordinates, (b) the LCO and the meshes in local coordinates system using 3 boundary elements and 7 control points, (c) triangular time-history of the dynamic loading

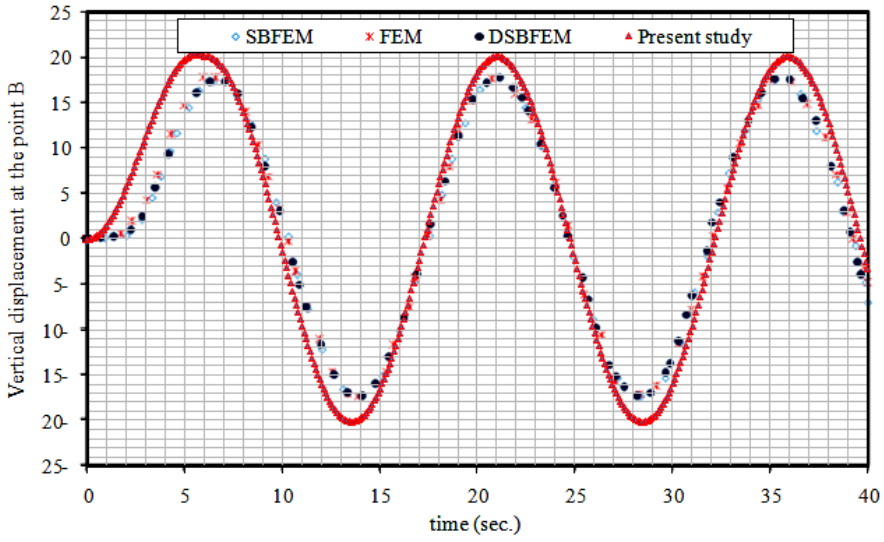

(a)

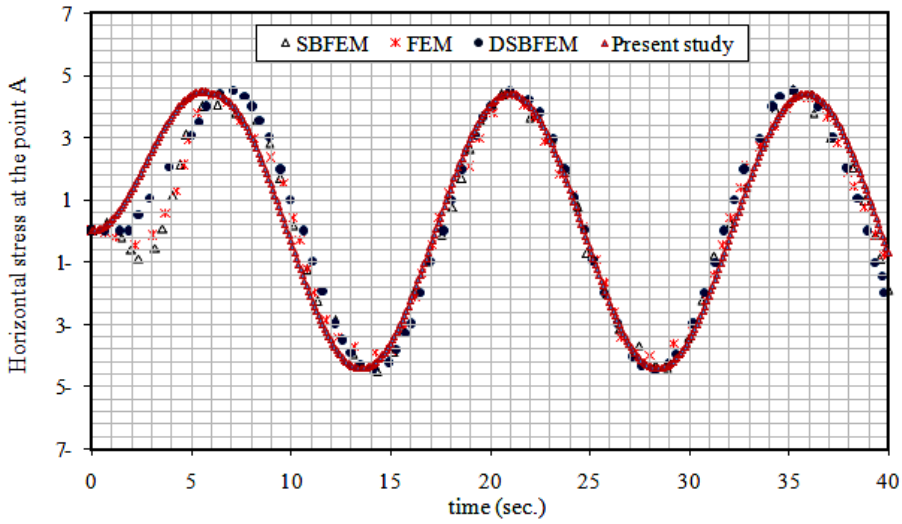

(b)

Figure 12. Results for the third example: (a) Vertical displacement at point B, (b) horizontal stress at point A; these results are from FEM, SBFEM [41], DSBFEM [46] and the proposed techniques in this study

5.4 Bi-material rectangular plate subjected to high-frequency load

In order to check the accuracy and efficiency of the present method in the analysis of impact problems, a rectangular plate consisting of two different materials (a steel- aluminum plate) loaded by a sinusoidal high-frequency loading (Fig. 13), is studied as the second elastodynamic example. Here, L=50*mm* and the maximum stress is 100 MPa at the time $t = 1.975 \times 10^{-6}$ sec. The steel material properties is with Young's modulus $E_{st} = 200\ GPa$, $\rho_{st} = 7860\ kg/m^3$ and the aluminum properties is with Young's modulus $E_{Al} = 70\ GPa$, $\rho_{Al} = 2710\ kg/m^3$ and also the Poisson's ratio of both material is zero to impose one-dimensional condition. The LCO is selected at the bottom of materials interface line as shown in Fig. 13. The corresponding boundaries are discretized employing 4 three-node elements with only 9 nodes and 18 DOFs in where, the maximum distance between the nodes is 12.5 *mm*; this element size is chosen because the minimum wave length of two materials under the present load is equal to 100.18 *mm*.

The time histories of variation of the horizontal displacement at point *A* calculated by the present method is shown in Fig. 14, in which other numerical and analytical solutions are also presented for comparison; this comparison shows a good agreement between the results; where, the proposed method is solved this problem using only 18^{th} DOF and in a very simple manner.

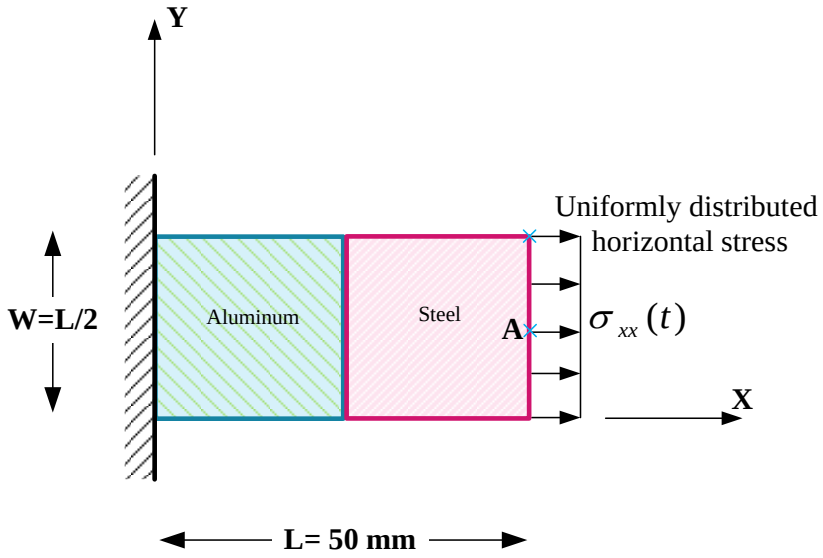

(a)

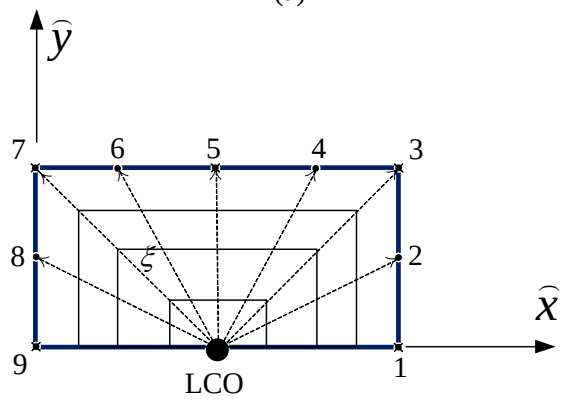

(b)

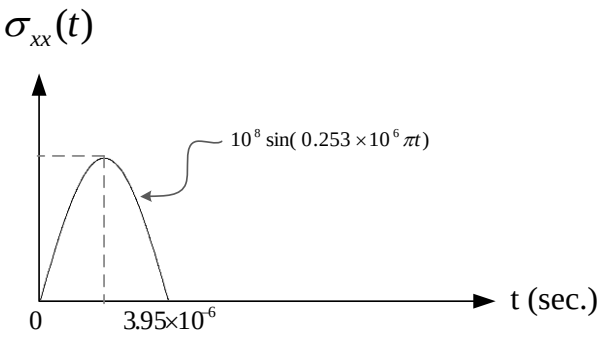

(c)

Figure 13. Fourth example: a Bi-material rectangular plate under dynamics excitation; (a) geometry and boundary conditions in global Cartesian coordinates, (b) the location of the LCO and the meshing in local coordinates system, (c) sinusoidal dynamic impulse

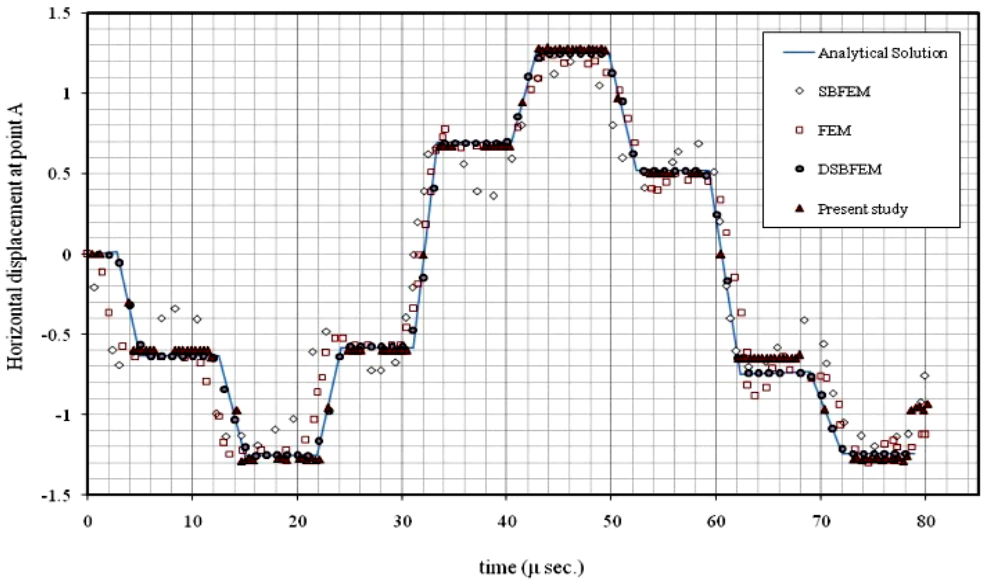

Figure 14. The variations of horizontal displacement at point A under the sinusoidal loading for the fourth example; Analytical solution, FEM, SBFEM [41], DSBFEM [46] and the present technique

5.5 Plane portal frame under a lateral dynamic load

In the last example, a two-dimensional plane-stress portal frame is considered to demonstrate the applicability of the proposed method in modeling structures that are more realistic. The geometry of this example is as illustrated in Fig. 15 and with Young's modulus $E = 100\ kPa$, density $\rho = 1\ kg/m^3$, and Poisson's ratio $\nu = 0.2$. This plate is fixed at the two bottom sides and is loaded by a uniformly distributed ramp dynamic lateral load as depicted in Fig. 15.

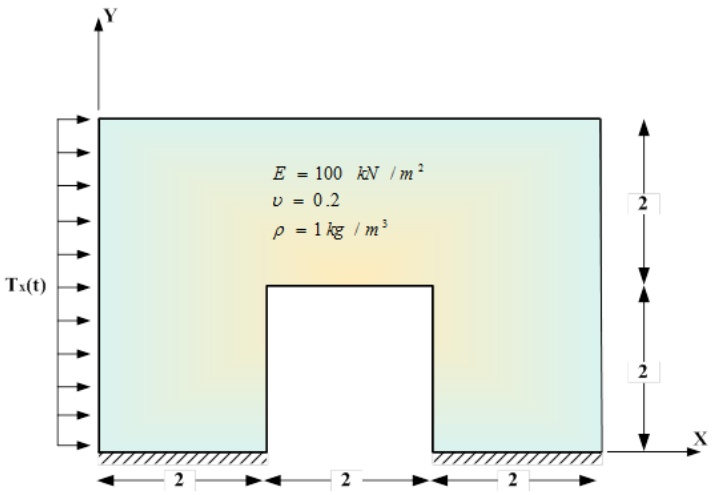

(a)

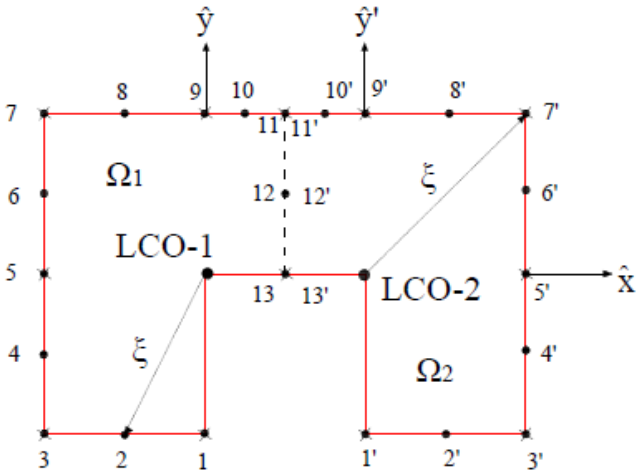

(b)

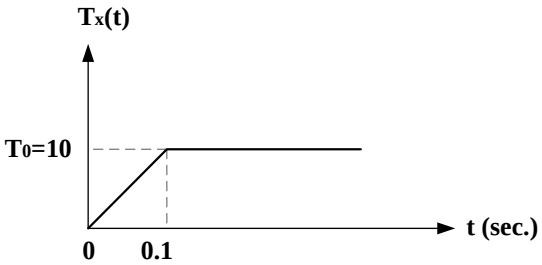

(c)

Figure 15. The 5th example is the portal frame subjected to lateral time-dependent load; (a) geometry and boundary conditions in global Cartesian coordinates, (b) the place of the LCOs and the proposed mesh employing three-node elements with 26 control points for each sub-domain and total 52 DOFs, in local coordinates system, (c) ramp function dynamic loading

The domain of this example is categorized as a concave geometry, where, not all the boundaries of the domain are visible from a unique point as LCO; so in these cases, the concave domain will be subdivided in some convex domains with their own local coordinate origin. Consequently, for the nodes located at the interface of new sub-domains, the compatibility and equilibrium conditions for displacement components and stress components, respectively, should be satisfied. The domain of the problem is subdivided in two sub-domains (Ω_1 and Ω_2 separated by a vertical dashed-line in Fig. 15, then two LCO are placed at the points where are shown in this figure. The boundaries of each sub-domain, which do not pass through the LCO, are discretized using a series of three-node element with total 13 nodes and 26 DOFs. The element size for this discretization is chosen 2 *m*, because the wavelength in this example regarding the material properties and dominant frequency of the load is more than 4.2 *m*.

The time variation of horizontal displacement at node 11(and/or node 11') is shown in Fig. 16. As shown in the figure, the results from the present method show good agreement with the results of other numerical methods and the proposed method is solved this example regarding a few number of DOF.

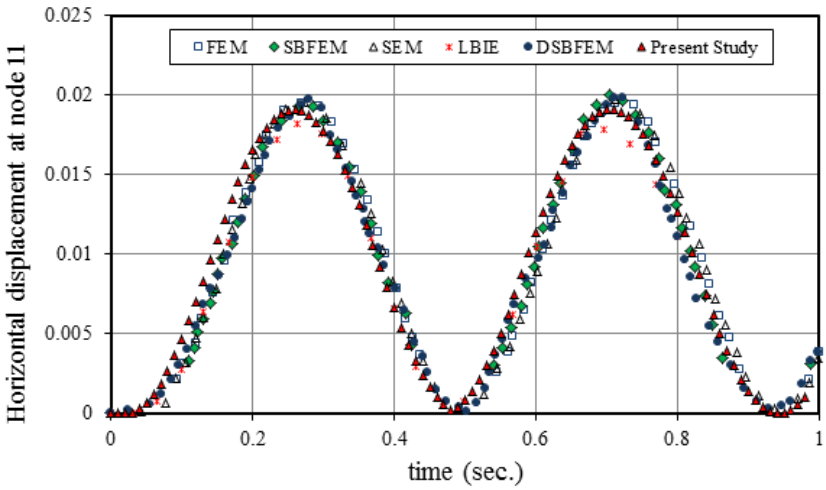

Figure 16. Horizontal displacement at node 11 (or 11') in the last example under the ramp time-dependence loading; from FEM, SBFEM [41], SEM, LBIE, DSBFEM [46] and the present technique

6. CONCLUSIONS

In this research, a modification on the novel semi-analytical method based on the scaled boundary-finite element method that is called as DSBFEM has been studied. The procedure of the modeling and solution of the 2D elastostatic and elastodynamic problems are similar to the DSBFEM. The difference in the proposed approach is that the boundary of the domain was discretized by new higher-order sub-parametric elements with Lagrange polynomials as mapping functions and the control points were Gauss-Lobatto-Legendre points, and also, using Gauss-Lobatto-Legendre quadrature the coefficient matrices of equations system became diagonal. This leads to a system of decoupled governing equations for the entire system. Five examples were successfully analyzed using the new proposed technique. In these examples, various elastostatic and elastodynamic problems and boundary conditions and various loading types were selected to show the generality and applicability of the present approach. It should be mentioned that all the examples were successfully modeled with very small number of DOFs and less complexity, preserving very high accuracy compared to the available analytical and numerical solutions.

REFERENCES

1. Zienkiewicz OC, Taylor RL. *The Finite Element Method*, Butterworth Heinemann, 2000.
2. Freitas JAT, Wang ZM. Elastodynamic analysis with hybrid stress finite elements, *Computers and Structures*, **79**(2001) 1753-67.

3. Khaji N, Habibi M, Mirhashemian P. Modeling transient elastodynamic problems using spectral element method, *Asian Journal of Civil Engineering*, No.4, **10**(2009) 597-617.
4. Khaji N, Kazemi Noureini H. Detection of a through-thickness crack based on elastic wave scattering in plates, Part I: forward solution, *Asian Journal of Civil Engineering*, No.13, **3**(2012) 305-322.
5. Kazemi Noureini H, Khaji N. Detection of a through-thickness crack based on elastic wave scattering in plates, Part II: inverse solution, *Asian Journal of Civil Engineering*, No.13, **4**(2012) 433-454.
6. Loureiro FS, Mansur WJ. An efficient hybrid time-Laplace domain method for elastodynamic analysis based on the explicit Green's approach, *International Journal of Solids and Structures*, **46**(2009) 3093-102.
7. Salvadori A. Analytical integrations in 2D BEM elasticity, *International Journal for Numerical Methods in Engineering*, **53**(2002) 1695-719.
8. Zhang X, Zhang X. Exact integration in the boundary element method for two-dimensional elastostatic problems, *Engineering Analysis with Boundary Elements*, **27**(2003) 987-97.
9. Zhang X, Zhang X. Exact integrations of two-dimensional high-order dis- continuous boundary elements of elastostatics problems, *Engineering Analysis with Boundary Elements*, **28**(2004) 725-32.
10. Kontoni DPN, Partridge PW, Brebbia CA. The dual reciprocity boundary element method for the eigenvalue analysis of Helmholtz problems, *Engineering Analysis with Boundary Elements*, **13**(1991) 2-16.
11. Vodicka R, Mantic V, Paris F. On the removal of the non-uniqueness in the solution of elastostatic problems by symmetric Galerkin BEM, *International Journal for Numerical Methods in Engineering*, **66**(2006) 1884-912.
12. Terravecchia S. Closed form coefficients in the symmetric boundary element approach, *Engineering Analysis with Boundary Elements*, **30**(2006) 479-88.
13. Chien CC, Wu TY. A particular integral BEM/time-discontinuous FEM methodology for solving 2-D elastodynamic problems, *International Journal of Solids and Structures*, **38**(2001) 289-306.
14. Yu G, Mansur W, Carrer JAM, Lie ST. A more stable scheme for BEM/FEM coupling applied to two-dimensional elastodynamics, *Computers and Structures*, **79**(2001) 811-23.
15. Chien CC, Chen Y, Chuang CC. Dual reciprocity BEM analysis of 2D transient elastodynamic problems by time-discontinuous Galerkin FEM, *Engineering Analysis with Boundary Elements*, **27**(2003) 611-24.
16. Soares DJ. A time-marching scheme based on implicit Green's functions for elastodynamic analysis with the domain boundary element method, *Computational Mechanics*, **47**(2007) 827-35.
17. Soares DJ, Mansur WJ. An efficient stabilized boundary element formulation for 2D time-domain acoustics and elastodynamics, *Computational Mechanics*, **49**(2007) 355-65.
18. Soares DJ, Mansur WJ, Estorff OV. An efficient time-domain FEM/BEM coupling approach based on FEM implicit Green's functions and truncation of BEM time convolution process, *Computer Methods in Applied Mechanics and Engineering*, **196** (2007) 1816–1826.
19. Abreu AI, Mansur WJ, Canelas A. Computation of time and space derivatives in a

CQM-based BEM formulation, *Engineering Analysis with Boundary Elements*, **33**(2009) 314-21.
20. Carrer JAM, Mansur WJ, Vanzuit RJ. Scalar wave equation by the boundary element method: a D-BEM approach with non-homogeneous initial conditions, *Computational Mechanics*, **44**(2009) 31-44.
21. Soares DJ, Mansur WJ. An efficient time-truncated boundary element formulation applied to the solution of the two-dimensional scalar wave equation, *Engineering Analysis with Boundary Elements*, **33** (2009) 43-53.
22. Gu YT, Liu GR. A meshless local Petrov-Galerkin (MLPG) method for free and forced vibration analysis for solids, *Computational Mechanics*, **27**(2011) 188-98.
23. Moosavi MR, Khelil A. Finite volume meshless local Petrov–Galerkin method in elastodynamic problems, *Engineering Analysis with Boundary Elements*, **33**(2009) 1016-21.
24. Liew KM, Cheng Y. Complex variable boundary element-free method for twodimensionalelastodynamic problems, *Computer Methods in Applied Mechanics and Engineering*, **198**(2009) 3925-33.
25. Liu GR, Gu YT. Comparisons of two meshfree local point interpolation methods for structural analyses, *Computational Mechanics*, **29**(2002) 107-21.
26. Sellountos EJ, Polyzos D. A meshless local boundary integral equation method for solving transient elastodynamic problems, *Computational Mechanics*, **35**(2005) 265-76.
27. Sadeghirad AR, Mahmoudzadeh Kani A, Rahimian M, Astaneh AV. A numerical approach based on the meshless collocation method in elastodynamics, *Acta Mechanica Sinica*, **25**(2009) 857-70.
28. Sellountos EJ, Polyzos D. A MLPG (LBIE) approach in combination with BEM, *Computer Methods in Applied Mechanics and Engineering*, **194**(2005) 859-875.
29. Zhang BR, Rajendran S. 'FE-Meshfree' QUAD4 element for free-vibration analysis, *Computer Methods in Applied Mechanics and Engineering*, **197**(2008) 3595-3604.
30. Liu Y, Belytschko T. A new support integration scheme for the weakform in mesh-free methods, *International Journal for Numerical Methods in Engineering*, **82**(2010) 699-715.
31. Wolf JP. *The Scaled Boundary Finite Element Method*, John Wiley & Sons, 2004.
32. Deeks AJ, Wolf JP. A virtual work derivation of the scaled boundary finite- element method for elastostatics, *Computational Mechanics*, **28**(2002) 489-504.
33. Yang ZJ, Deeks AJ, Hao H. A Frobenius solution to the scaled boundary finite element equations in frequency domain for bounded media, *International Journal for Numerical Methods in Engineering*, **70**(2007) 1387-1408.
34. Bazyar MH, Song C. Time-harmonic response of non-homogeneous elastic unbounded domains using the scaled boundary finite-element method, *Earthquake Engineering & Structural Dynamics Journal*, **35**(2006) 357-83.
35. He Y, Yang H, Xu M, Deeks AJ. A scaled boundary finite element method for cyclically symmetric two-dimensional elastic analysis, *Computers & Structures*, **12**(2013) 1-8.
36. Bird GE, Trevelyan J, Augarde CE. A coupled BEM/scaled boundary FEM formulation for accurate computations in linear elastic fracture mechanics, *Engineering Analysis with Boundary Elements*, **34**(2010) 599-610.

37. Deeks AJ, Augarde CE. A meshless local Petrov-Galerkin scaled boundary method, *Computational Mechanics*, **36**(2005) 159-70.
38. Chen X, Birk C, Song C. Transient analysis of wave propagation in layered soil by using the scaled boundary finite element method, *Computers and Geotechnics*, **63**(2015) 1-12.
39. Chen C, Birk C, Song C. Numerical modelling of wave propagation in anisotropic soil using a displacement unit-impulse-response-based formulation of the scaled boundary finite element method, *Soil Dynamics and Earthquake Engineering*, **65**(2014) 243-55.
40. Khaji N, Mirzajani M. Frequency domain analysis of elastic bounded domains using a new semi-analytical method, *Acta Mechanica*, **224**(2013) 1555-70.
41. Natarajan S, Ooi ET, Chiong I, Song C. Convergence and accuracy of displacement based finite element formulations over arbitrary polygons: Laplace interpolants, strain smoothing and scaled boundary polygon formulation, *Finite Elements in Analysis and Design*, **85**(2014) 101-22.
42. Natarajan S, Wang J, Song C, Birk C. Isogeometric analysis enhanced by the scaled boundary finite element method, *Computer Methods in Applied Mechanics and Engineering*, **283**(2015) 733-62.
43. Hea Y, Yanga H, Deeks AJ. Use of Fourier shape functions in the scaled boundary method, *Engineering Analysis with Boundary Elements*, **41**(2014) 152-9.
44. Khaji N, Khodakarami MI. A new semi-analytical method with diagonal coefficient matrices for potential problems, *Engineering Analysis with Boundary Elements*, **35**(2011) 845-54.
45. Khodakarami MI, Khaji N. Analysis of elastostatic problems using a semi-analytical method with diagonal coefficient matrices, *Engineering Analysis with Boundary Elements*, **35**(2011) 1288-96.
46. Khodakarami MI, Khaji N, Ahmadi MT. Modeling transient elastodynamic problems using a novel semi-analytical method yielding decoupled partial differential equations, *Computer Methods in Applied Mechanics and Engineering*, **213-216**(2012) 183-95.
47. Khaji N, Khodakarami MI. A semi-analytical method with a system of decoupled ordinary differential equations for three-dimensional elastostatic problems, *International Journal of Solids and Structures*, **49**(2012) 2528-46.
48. Khodakarami MI, Khaji N. Wave propagation in semi-infinite media with topographical irregularities using Decoupled Equations Method, *Soil Dynamics and Earthquake Engineering*, **65**(2014) 102-12.
49. Canuto C, Hussaini MY, Quarteroni A, Zeng TA. *Spectral Methods in Fluid Dynamics*, Springer, 1988.
50. Lebedev NN. *Special functions and their applications*. Prentice-Hall; 1965.